# Synthesis and characterization of rod-like ZnO decorated with gamma-Fe2O3 nanoparticles monolayer

Imen Balti, Laila Samia Smiri, Pierre Rabu, Eric Gautron, Bruno Viana, Noureddine Jouini

# Synthesis and characterization of rod-like ZnO decorated with $\gamma$-$Fe_2O_3$ nanoparticles monolayer

Imen Balti [a,b,*], Laila Samia Smiri [a], Pierre Rabu [c], Eric Gautron [d], Bruno Viana [e], Noureddine Jouini [b]

[a] Unité de Recherche 99/UR12-30, Faculté des Sciences de Bizerte, Université de Carthage, 7021 Jarzouna, Tunisia
[b] Laboratoire des Sciences des Procédés et Matériaux, LSPM, CNRS, UPR 3407, Université Paris XIII, 99 Avenue J.B. Clément, 93430 Villetaneuse, France
[c] Département de Chimie des Matériaux Inorganiques, IPCMS, UMR 7504, CNRS–UDS, 23, rue du Loess, BP 43, Strasbourg Cedex 2, France
[d] Institut des Matériaux Jean Rouxel (IMN)-UMR 6502, Université de Nantes, CNRS, 2 rue de la Houssinière, BP 32229, 44322 Nantes Cedex 3, France
[e] LCMCP, Chimie-Paristech, UPMC, Collège de France, UMR CNRS 7574, 11 rue Pierre et Marie Curie, 75005 Paris, France

Decorated rod-like ZnO particles with $\gamma$-$Fe_2O_3$ nanoparticles monolayer (ZnO@$\gamma$-$Fe_2O_3$) were prepared via a simple route using forced hydrolysis of metal acetates in a polyol medium. The phases and purity of the as-prepared particles were established by powder X-ray diffraction (PXRD) and X-ray photo-electron spectroscopy (XPS) analyses. Transmission electron microscopy (TEM) showed that the ZnO particles present a typical rod-like morphology with ~80 nm diameter and ~200–400 nm length. These nanorods are decorated with well-organized $\gamma$-$Fe_2O_3$ spherical nanoparticles showing a narrow size distribution around 5 nm. The photoluminescence (PL) spectra of the bare ZnO particles show predominant UV-excitonic and weak visible emission. The latter vanishes after covering the surface with the $\gamma$-$Fe_2O_3$ nanoparticles suggesting an effect on the oxygen stoichiometry at the surface of the ZnO nanorods. The decorated nanoparticles exhibit magnetic response to an external magnetic field at room temperature and a superparamagnetic character with very low blocking temperature likely related to the organisation of $\gamma$-$Fe_2O_3$ nanoparticles as monolayer.

## 1. Introduction

During the past decades, ZnO-based magnetic semiconductors (MSs) have gained a significant attraction because of their unique properties with possible technological applications utilizing both the semiconductor physics and the ferromagnetism [1]. However, in spite of the large number of groups which have been interested by this subject, the existence of ferromagnetism (FM) at room temperature in 3d metal doped zinc oxide remains unproved and the results are sometimes contradictory [2–4]. Alternatively, ZnO-based MS could also be achieved by fabricating core@shell or composite nanoparticles. In the whole system, the semiconducting properties might be provided by the ZnO part while magnetic properties could be obtained by the magnetic part. Therefore, these composite nanostructures are good candidates for applications in the field of medical sciences and biotechnologies [5–8]. In this context, many efforts have been devoted to fabricate core@shell systems based on ZnO and superparamagnetic iron oxide nanoparticles [9–11], like ZnO@$Fe_3O_4$ and $Fe_3O_4$@ZnO [12,13]. In these systems, the ZnO can present an equiaxed or uni-axed shape and the iron oxide can be maghemite or magnetite phase. For example, Jing et al. have synthesized core@shell zinc oxide@magnetite (ZnO@$Fe_3O_4$) with tubular morphology [14]. Jiaqi et al. reported on the synthesis of spherical core@shell magnetite@zinc oxide ($Fe_3O_4$@ZnO) [15]. ZnO nanorods decorated with $\gamma$-$Fe_2O_3$ have been obtained via several steps by Wu et al. [11]. First ZnO nanorods are elaborated by a seed-assisted chemical reaction and then modified by polyelectrolytes via layer-by layer assembly. The as-modified nanorods are then decorated with iron oxide nanoparticles by chemical reaction using $FeCl_3{\cdot}6H_2O$ and $NaBH_4$ as reactants [11,16].

In our study, we present an alternative approach to elaborate rod-like ZnO decorated with $\gamma$-$Fe_2O_3$. It consists of a one-pot simple method using forced hydrolysis of acetate metallic salts in a polyol medium. This allowed us to obtain ZnO nanorods decorated with monolayer $\gamma$-$Fe_2O_3$ nanoparticles. The optical and magnetic properties of the as-synthesized particles have been investigated in relation to their morphologies and in regard to electron transmission microscopy results. In comparison with the above cited results, the as-obtained system presents very few defects on ZnO nanorods and low dipolar interactions between iron oxide

* Corresponding author at: Laboratoire des Sciences des Procédés et Matériaux, LSPM, CNRS, UPR 3407, Université Paris XIII, 99 Avenue J.B. Clément, 93430 Villetaneuse, France. Tel.: +33 149403388; fax: +33 149403938.
*E-mail address:* imenbalti12@yahoo.fr (I. Balti).

nanoparticles. This leads to excellent UV photoluminescence properties along with superparamagnetic behavior with very low blocking temperature.

## 2. Experimental section

### 2.1. Synthesis of ZnO@$\gamma$-$Fe_2O_3$

To synthesize the rod-like ZnO decorated with $\gamma$-$Fe_2O_3$ nanoparticles, zinc acetate dihydrate ($Zn(Ac)_2{\cdot}2H_2O$), sodium acetate trihydrate ($Na(Ac){\cdot}3H_2O$) (13.61 g) and distilled water (18 ml) were successively dissolved in 50 ml of diethylene glycol (DEG) sonicated for 30 min and then heated to reflux (245 °C) during 4 h. After cooling down to room temperature a white homogeneous suspension was obtained. Then the solution of iron acetate ($Fe(Ac)_2$) in DEG was injected into the suspension obtained above, and the mixture was slowly heated to 245 °C and maintained at this temperature for about 4 h. The dark brown powder was then separated from the supernatant by centrifugation, after slow cooling to room temperature, washed several times in ethanol and acetone and then dried in vacuum at 50 °C.

The Fe/Zn ratio has been varied in this study resulting in nanorods decorated with different amounts of $\gamma$-$Fe_2O_3$ particles as summarized in Table 1.

### 2.2. Characterization techniques

The chemical analysis of metal elements was conducted at the CNRS central analysis service at Solaize using Inductively Coupled Plasma–Atomic Emission Spectroscopy (ICP–AES).

X-ray diffraction patterns of the powders were recorded using an INEL diffractometer with a copper anticathode with Cu K$\alpha$ ($\lambda$ = 1.5405 Å) radiation. The crystalline phases were identified using the Match software [17]. The refinement of the unit cell parameters was carried out by the Rietveld method [18] from the PXRD diffractograms using the Fullprof program [19]. The average crystallites' sizes were, finally, calculated by using the Scherrer's formula based on the width of intense diffraction peaks.

Transmission electron microscopy (TEM) observations were made with a Hitachi H-9000 NAR (300 kV, Scherzer resolution 0.18 nm).

Photoluminescence (PL) measurements were carried out at room temperature. The excitation source at 266 nm was provided by a frequency quadrupled Nd:YAG (10 ns, 10 Hz). The emission was analyzed by using a HR250 monochromator (Jobin–Yvon) coupled with a UV-enhanced intensified charge coupled device (ICCD, Roper). Under pulsed laser excitation, luminescence spectra were recorded with an intensity integration over 300 ms corresponding to the integration of the intensity for three UV excitation pulses. The excitation power and the geometrical arrangement of the experimental setup were kept unchanged for all samples.

A Quantum Design S-VSM superconducting quantum interference device (SQUID) magnetometer was used to measure the magnetic properties of nanoparticles. The hysteresis loops were recorded at 2 K and 300 K in the range −7T to +7T. The thermal variation of the magnetization was studied in the zero-field-cooled/field-cooled (ZFC/FC) mode under an applied magnetic field of 100 Oe, between 1.8 K and 300 K. AC susceptibility measurements were carried out in 3.5 Oe–83 Hz alternative field.

X-ray photoelectron spectroscopy (XPS) was carried out with a PHI 5600-ci spectrometer (Physical Electronics, Eden Prairie, MN, USA). The anode used is Al monochromatic (1486.6 eV) at 300 W.

## 3. Results and discussion

Chemical analysis by ICP indicated that the molar ratio of Fe/Zn in samples ZF1, ZF2 and ZF3 are much closer to initial ones (Table 1).

### 3.1. Powder X-ray diffraction

Fig. 1 shows the PXRD pattern of as prepared nanoparticles with different metal ratio. Compared with data reported in JCPD No. 99-101-2013 [17], all peaks marked by asterisks (∗) correspond to the cubic iron oxide phases or to $ZnFe_2O_4$. Indeed these three compounds belong to the inverse spinel structure with the same space group Fd-3m and with cell constant varying in a narrow range (0.844–0.840 nm) [20]. The other peaks marked by losanges (♦) can be indexed with the hexagonal wurtzite ZnO cell constants $a$ = 0.323 nm and $c$ = 0.520 nm (JCPDS 99-100-4744)[17]. The results suggest that the composites were formed of iron oxide or zinc ferrite along with zinc oxide with no extra phases. The size of each type of crystallites ($L_{XRD}$) was estimated from the FWHM of the (311) peak of the iron oxide, (002) and (100) peaks of ZnO. The values deduced from the Scherrer formula are 5.1 ± 0.5 nm for iron oxide and 75.2 ± 0.4 nm corresponding to (002) and 53.8 ± 0.4 nm corresponding to (100) for the zinc oxide.

The PXRD is not an ideal method to differentiate crystalline forms of iron-oxide $\gamma$-$Fe_2O_3$ (maghemite), $Fe_3O_4$ (magnetite), and $ZnFe_2O_4$ (zinc ferrite). Moreover, the small particle size leads to the broadening of the diffraction peaks which makes a precise analysis of the diffraction profile more difficult.

### 3.2. X-ray photoelectron spectroscopy analyses

Therefore, X-ray photoelectron spectroscopy analysis was used to differentiate between the three phases [20–22]. The XPS spectrum of each sample (Fig. 2) exhibits two main peaks at about 711 and 725 eV corresponding to Fe $2p_{3/2}$ and Fe $2p_{1/2}$ and satellite peaks at 719.1 and 733.4 eV, indicated by red arrows, at the higher binding energy sides of the main peaks. These two peaks can be attributed without ambiguity to compounds containing ferric ion [22]. Thus the compounds present in the samples can be $\gamma$-$Fe_2O_3$ or $ZnFe_2O_4$. This result is in good agreement with reported studies on heterostructured composites based on ZnO and iron oxides [9–11]. As it will be discussed hereafter, the existence of $ZnFe_2O_4$ can be ruled out on the basis of the synthesis conditions and the related growth mechanism of the core-shell nanocomposites formation.

### 3.3. TEM characterization

Fig. 3 presents a typical transmission electron microscope (TEM) image of as-synthesized ZnO particles before and after coating. The ZnO particles prepared in polyol medium cristallize as nanorods with size of ∼80 nm in diameter and ∼200–400 nm in length. They have a smooth and homogenous surface (Fig. 3A (left panel)). This result is in good agreement with the previous work of Dakhlaoui et al. [23]. The diameter fits well with the crystallite size deduced from the Scherrer formula applied to the (002) family of planes. The comparison of the nanorod length (200–400 nm) with the crystallite size corresponding to (100) peak (53.8 nm) may indicate the polycrystalline character of the nanorods. The exploration of several zones on the grid, shows that nucleation and growth of $\gamma$-$Fe_2O_3$ particles occurred on the ZnO nanorod surface resulting in a magnetic monolayer decorating the semi-conducting nanorods (Fig. 3B(a–c)). The $\gamma$-$Fe_2O_3$ nanoparticles have an almost spherical morphology with diameter of 5 ± 1 nm in good agreement with the

**Table 1**
Fe/Zn ratio, coercive field, maximum of magnetization at 2 K and blocking temperature of the as-prepared nanoparticles (ZF1, ZF2 and ZF3).

| | $Zn(Ac)_2{\cdot}2H_2O$ (mmol) | $Fe(Ac)_2$ (mmol) | $(Fe/Zn)_{th}$ | $(Fe/Zn)_{exp}$ | $H_c$ (Oe) | $M_{sat}$ (emu $g^{-1}$) | $M_{sat}$[a] | $T_B$ (K) |
|---|---|---|---|---|---|---|---|---|
| ZF1 | 2 | 2 | 1 | 0.84 | 7 | 1.66 | 2.18 | 6 |
| ZF2 | 2 | 4 | 2 | 1.75 | 44 | 0.40 | 0.63 | 5.9 |
| ZF3 | 2 | 8 | 4 | 3.90 | 63 | 1.75 | 2.20 | 6.5 |

th: Theory and exp: experimental.
[a] $M_{sat}$ (emu/$g_{\gamma\text{-}Fe_2O_3}$).

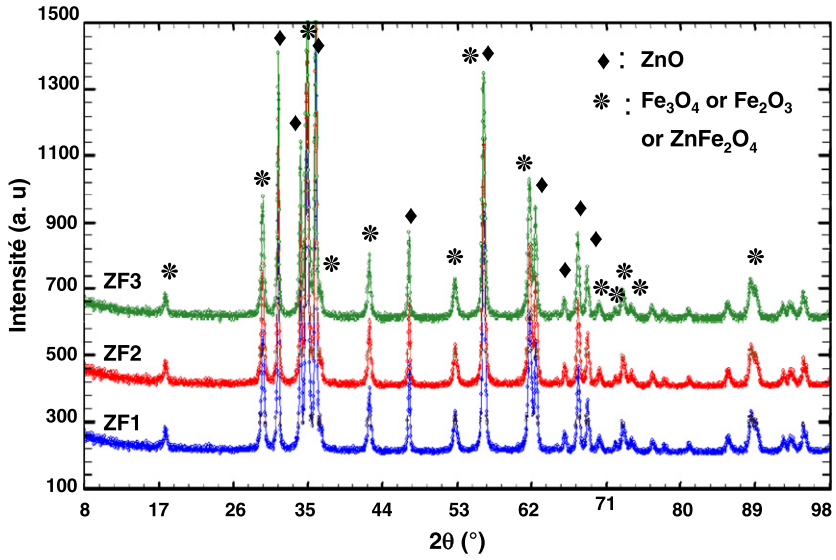


**Fig. 1.** Powder X-ray diffraction patterns of samples according to compositions indicated in Table 1. The square (♦) indicates zinc oxide with a wurtzite structure, and the asterisk (∗) indicates the maghemite ($\gamma$-$Fe_2O_3$) or magnetite ($Fe_3O_4$) phase or zinc ferrite ($ZnFe_2O_4$).

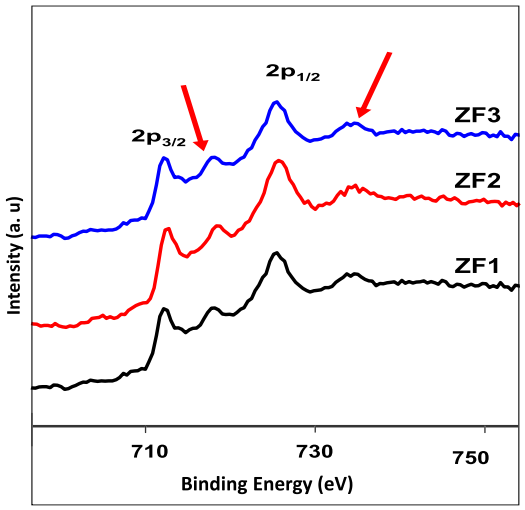


**Fig. 2.** The X-ray photoelectron spectroscopy spectra (XPS) of as prepared core@shell ZnO@$\gamma$-$Fe_2O_3$ nanoparticles. The XPS peaks indicated by red arrows are characteristic of $Fe^{3+}$. (For interpretation of the references to colour in this figure legend, the reader is referred to the web version of this article.)

crystallite size deduced from the PXRD pattern analysis. It should be noted that ZnO particles decorated with $\gamma$-$Fe_2O_3$ nanoparticles have been previously reported. Chu et al. [10] prepared ZnO microrods coated with iron oxide nanoparticles. Wu et al. [11] prepared ZnO nanorods coated with irregular agglomerated $\gamma$-$Fe_2O_3$ nanoparticles. In the present work, it was possible to control the amount of iron oxide deposited on ZnO nanorods succeeding in the formation of $\gamma$-$Fe_2O_3$ monolayer with well separated nanoparticles.

From high resolution TEM images (Fig. 3B(d)), one can notice a sharp interface between the ZnO core and the $\gamma$-$Fe_2O_3$ shell regions. Interplanar spaces of 0.237 and 0.476 nm were measured in the core and shell regions, corresponding respectively to ZnO (1 0 1) and $\gamma$-$Fe_2O_3$ (1 1 1) planes. Those results are in good agreement with the X-ray-diffraction patterns discussed above.

An HRTEM micrograph on coated particles is presented in Fig. 4. The Fast Fourier Transform (FFT) performed on one of those particles is presented in inset. This FFT can be simulated with the $\gamma$-$Fe_2O_3$ maghemite structure or with $ZnFe_2O_4$ one since these two compounds belong to cfc structure and present very close cell parameters as discussed above. However one can argue that due to the synthesis conditions, the hypothesis of particles containing only $ZnFe_2O_4$ is not consistent. Indeed, ZnO nanorods are formed prior to the addition of iron salt in the medium. Then iron precursor undergoes hydrolysis and polycondensation leading to the growth of $\gamma$-$Fe_2O_3$ nanoparticles on the nanorods surface which remains very regular. Obviously these reactions occurring in solution are more favoured than Zn diffusion from ZnO nanorods into the interface to form zinc ferrite. Our conclusion is in good agreement with several works describing the synthesis of ZnO nanorods decorated with $\gamma$-$Fe_2O_3$ nanoparticles free of $ZnFe_2O_4$. This does not exclude however that some Zn diffusion mechanism can lead to the formation of $ZnFe_2O_4$ over few atomic layers in the interface between ZnO nanorods and $\gamma$-$Fe_2O_3$ nanoparticles. However, the HRTEM image (Fig. 4) does not evidence the presence of a different structure at the interface.

### *3.4. Photoluminescence measurement*

Photoluminescence (PL) is a technique which can provide data related to defect levels, and the ratio $I_{UV}/I_{DL}$ (the intensity of the ultraviolet to the visible deep level related luminescence) is a measure of defect states in ZnO material. Fig. 5 shows the room temperature photoluminescence spectra of the ZnO@$\gamma$-$Fe_2O_3$ compared to that of the uncovered ZnO nanoparticles. All samples present the typical UV-exitonic emission band of ZnO. This emission occurs at 376 nm in bare ZnO whereas it is shifted to higher wavelength for the coated nanorods. Similar behavior was observed by Chu et al. for ZnO microrods coated with $\gamma$-$Fe_2O_3$ [10]. The bare ZnO nanorods also exhibit a broad DL band between 480 and 600 nm ascribed to defect processes [24–27]. The ratio $I_{UV}/I_{DL}$ is very high. This indicates the good crystallinity of the as-prepared nanorods and the presence of very low amount of defects in good agreement with results reported by Dakhaloui et al. [23]. For the core@shell nanorods one can note the vanishing of the DL bands. This suggests that growth and coating of ZnO with $\gamma$-$Fe_2O_3$ tends to minimize the defects. In the inset of Fig. 5, the visible emission of defects with kinetics in the range of the nanosecond scale is presented. The origin of the green emission in zinc oxide has remained controversial and it has been assumed that

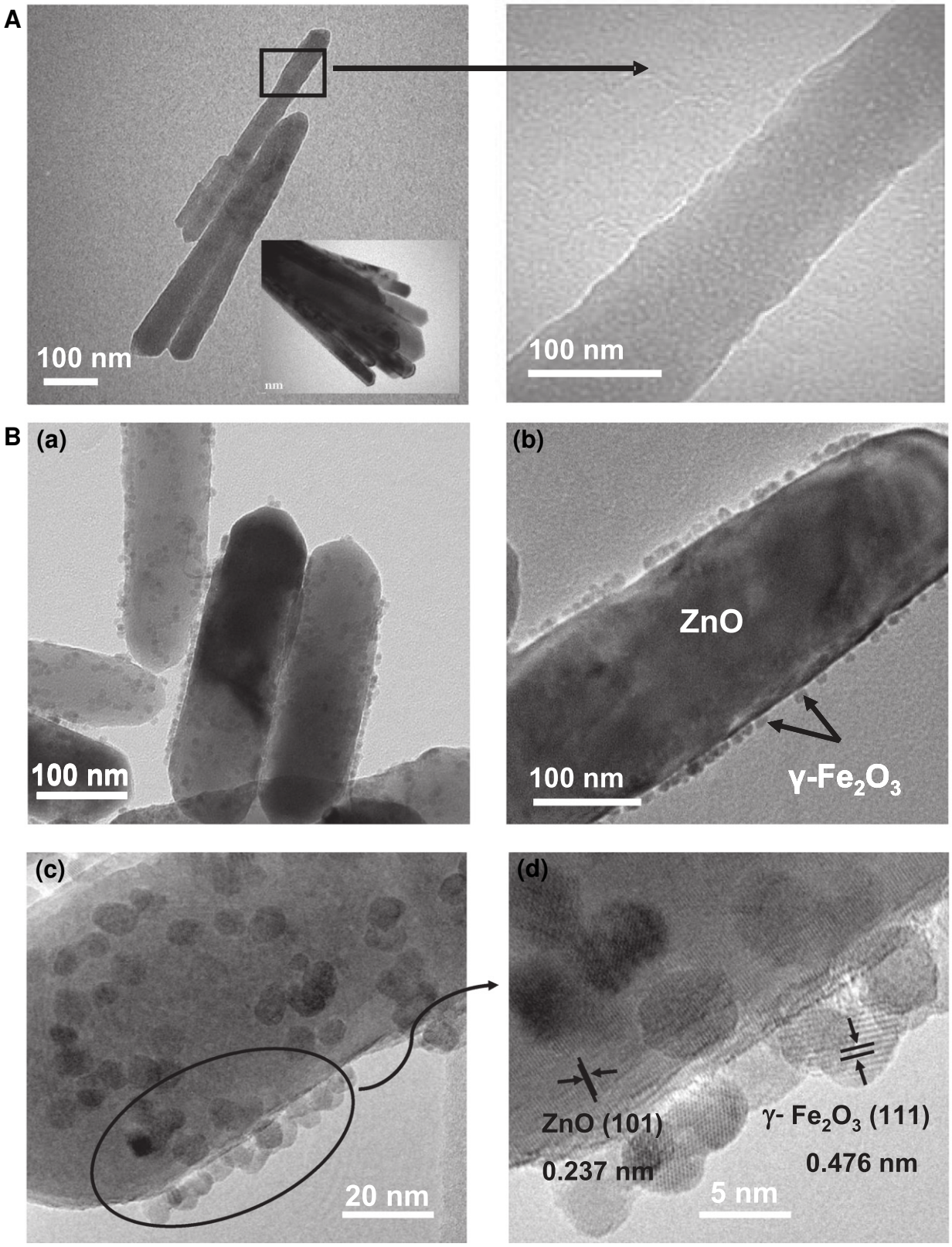


**Fig. 3.** TEM images of (A) rod like ZnO nanoparticles before coating, (B) after coating with $\gamma$-$Fe_2O_3$ (ZF2).

structural and surface defects as well as oxygen vacancies are responsible [28]. Similar results of a reduction of the defects bands after surface coating are presented in Refs. [10,11,29]. The significant decrease of surface defects results in the enhancement of the UV photoluminescence of the nanoparticles. However an opposite phenomenon was also observed for ZnO microrods coated

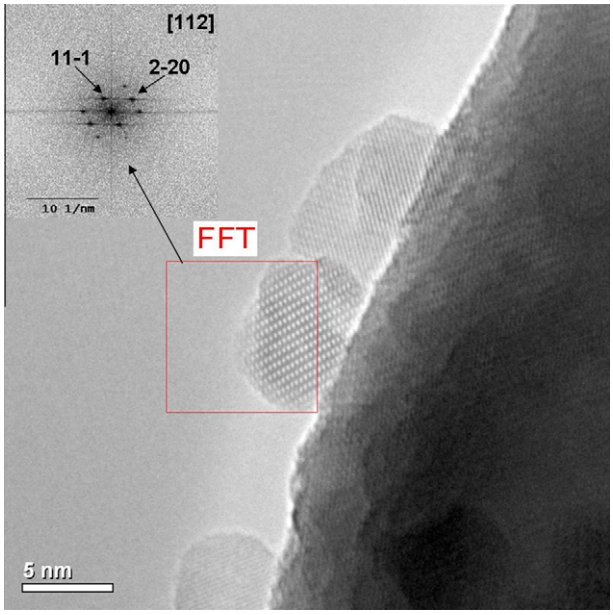


**Fig. 4.** HRTEM micrograph on coated particles of ZF2 sample with Fe/Zn ratio about 2. The Fast Fourier Transform (FFT) performed on one of those particles is presented in inset.

with $\gamma$-$Fe_2O_3$ where the DL band intensity increases in comparison with bare ZnO microrods [10].

### 3.5. Magnetic measurements

The as-prepared nanoparticles have the ability to accumulate near a commercial permanent magnet at room temperature. Fig. 6 presents the observation which demonstrate the sensitive magnetic response of ZF2 sample (Fe/Zn = 2) as an example.

The magnetic behavior of all samples was further investigated by means of field dependent and temperature dependent magnetic measurements. The variation of the magnetization as a function of the magnetic field (Fig. 7) of all decorated particles exhibits a linear variation of the moment with zero remanence or coercivity at

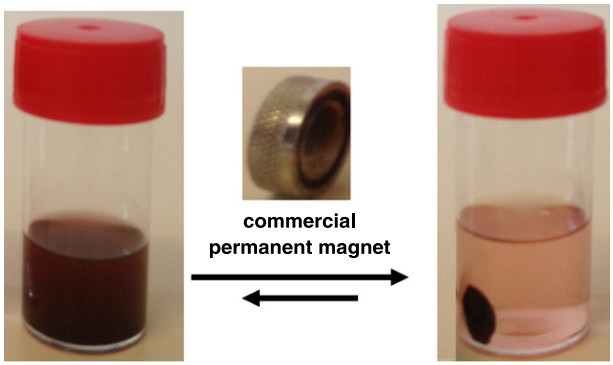


**Fig. 6.** Observation which demonstrates the ability of nanoparticles (ZF2) to accumulate near a commercial permanent magnet.

300 K. At 2 K, a hysteresis is observed for all nanocomposites indicating the existence of ferromagnetic order. The coercive fields and saturation magnetization values measured for all the samples are summarized in Table 1. The saturation magnetizations for all samples, not exceeding 3 emu per gram of $\gamma$-$Fe_2O_3$ are very low in comparison with that of bulk maghemite (82 emu/g) [30]. Saturation magnetizations lower than 20 emu/g have been reported for maghemite nanoparticles with size less than 6.6 nm. This reduction is a well-known behavior of ferrite nanoparticles generally ascribed to a magnetically disordered moments on their surface due to broken exchange bonds at the external layer as well as to structural defects inside the particles [31,32]. Fig. 7 also reveals that the magnetization at 2 K does not saturate even at high field of 7 T. This can be due to frozen spins at the surface as recently reported for maghemite nanoparticles with 4 nm in diameter obtained by microwave plasma method [33].

The thermal variation of the magnetic susceptibility is shown in Fig. 8. For all samples, ZFC and FC susceptibilities are superposed down to 6.0, 5.9 and 6.5 K for ZF1, ZF2 and ZF3 respectively. Below this temperature, irreversibility is observed. ZFC susceptibility continues to increase while FC susceptibility decreases.

Fig. 9 presents AC susceptibility measurements done under 3.5 Oe/83 Hz AC field. The three samples exhibit a sharp out of

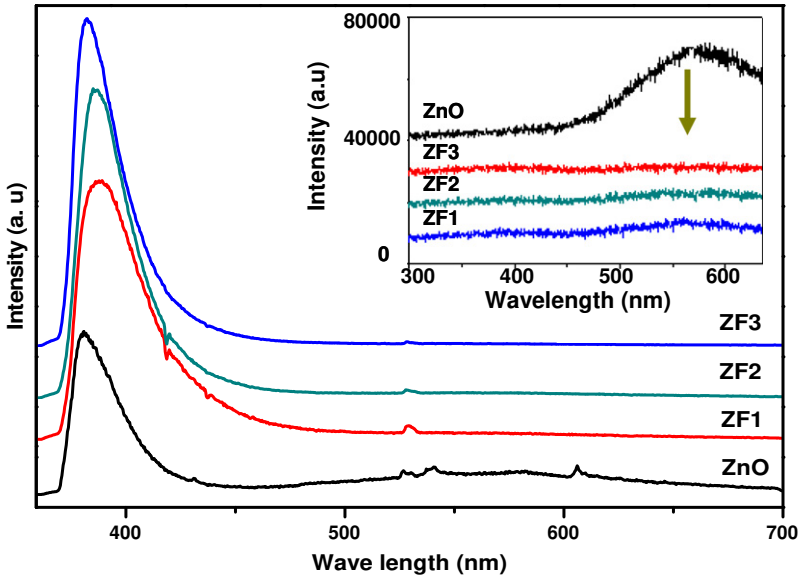


**Fig. 5.** Photoluminescence spectra of as prepared ZnO@$\gamma$-$Fe_2O_3$ (ZF1, ZF2 and ZF3 see Table 1) nanoparticles compared to that of rod like ZnO synthesized in polyol medium. Insert presented the emission after 26 ns delay. Only defects emissions are therefore visible.

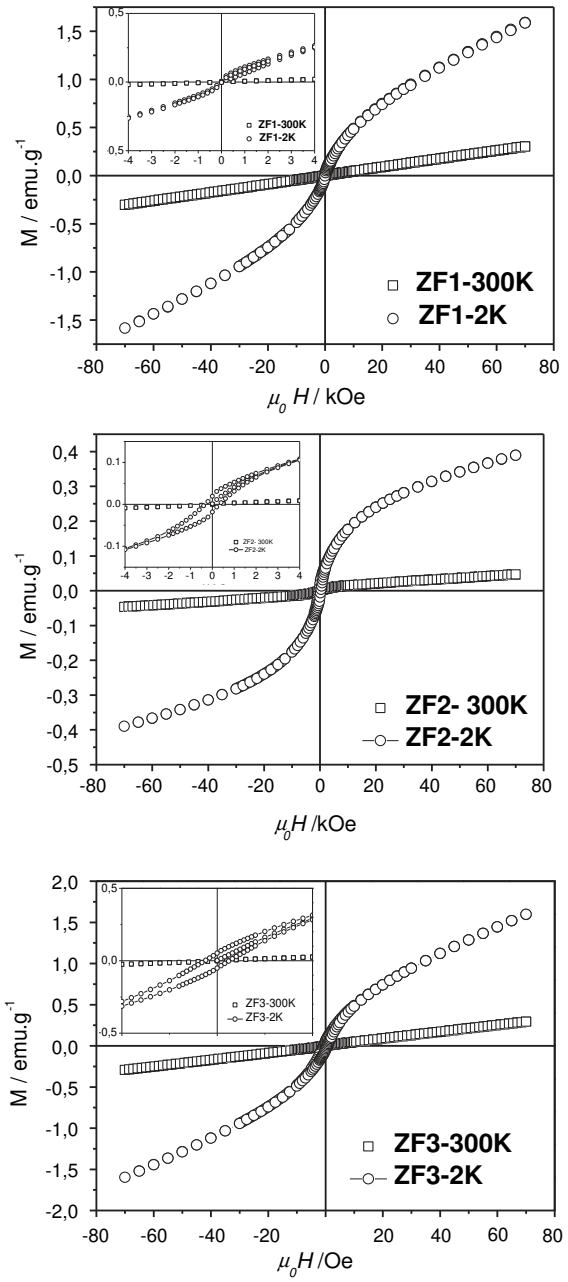


**Fig. 7.** Magnetization (M) versus applied field (H) curve of ZF1, ZF2 and ZF3 samples measured at 2 and 300 K. The magnetic hysteresis loop is clearly observed at 2 K resulting from ferromagnetic character (inset as a zoom).

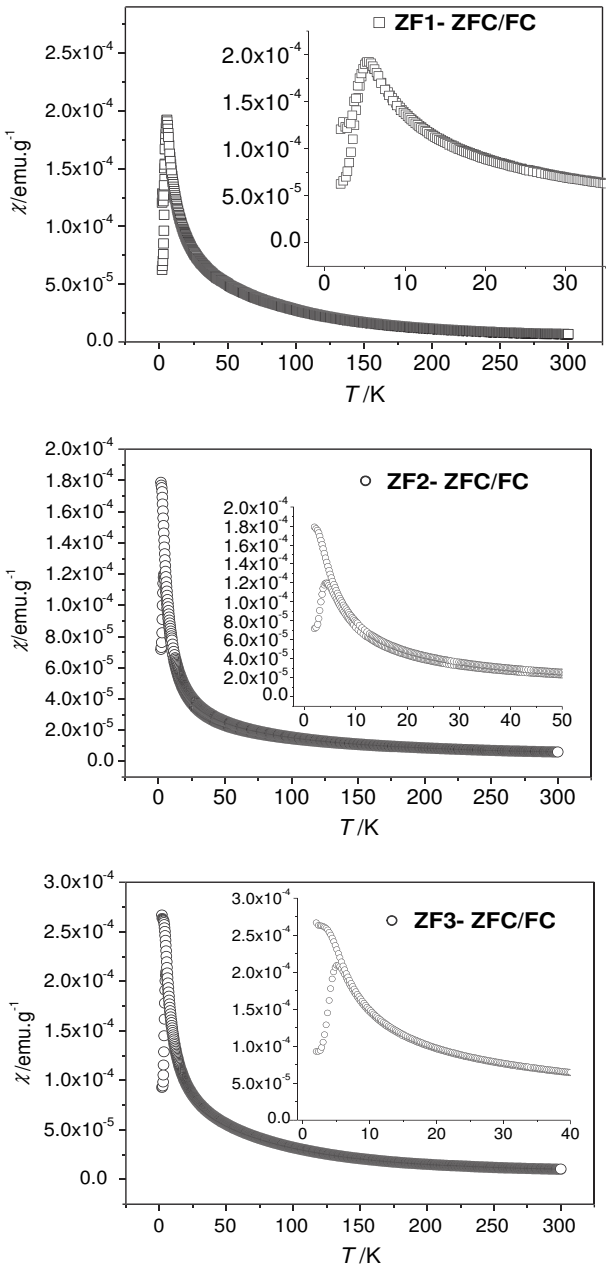


**Fig. 8.** Temperature-dependent susceptibility $\chi$ of ZF1, ZF2 and ZF3 nanoparticles at a magnetic field of 100 Oe (inset as a zoom).

phases signal at low temperature. This indicates a superparamagnetic behavior with a blocking temperature ($T_B$) in the range 5–6.5 K, as deduced from the maximum of the peak in the real part of the susceptibility. The sharpness of the peak of the ZFC curve below $T_B$ is consistent with narrow size distribution of the magnetic nanoparticles. It is interesting to note that $T_B$ depends not only on the particle size but also on magnetic interactions between nanoparticles as suggested by Monte Carlo simulations [34]. It was shown that strong interparticles interactions lead to a very high blocking temperature (300 K) for $\gamma$-$Fe_2O_3$ nanoparticles with 5.5 nm in diameter [35]. Such interparticles interactions can explain the ferromagnetic behavior observed in $\gamma$-$Fe_2O_3$ nanoparticles encapsulated in ZnO/ZnS nanoribbons [9]. Conversely, the very low values of $T_B$ observed in our case point to very weak dipolar interactions. This can stem from the fact that the magnetic particles are strongly bonded to ZnO nanorods and relatively separated from each other as observed by TEM.

## 4. Conclusion

In summary, ZnO nanorods uniformly decorated with $\gamma$-$Fe_2O_3$ were successfully synthesized using forced hydrolysis of acetate metallic salts in a polyol medium. First, ZnO nanorods with very low surface defects are obtained. Then, these nanorods act as seed for the growth of well-defined maghemite nanoparticles with 5 nm diameter. In comparison with similar systems reported in the literature, herein $\gamma$-$Fe_2O_3$ nanoparticles form a well-defined monolayer on the surface of ZnO nanorods. Photoluminescence study shows that the growth and coating of maghemite nanoparticles onto the

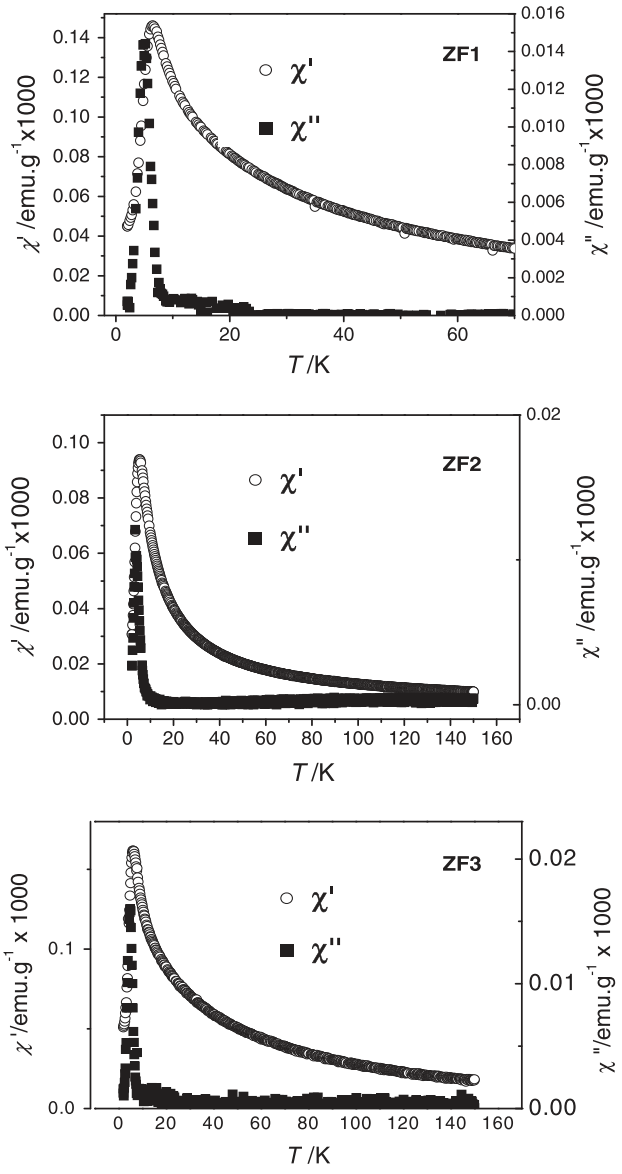


**Fig. 9.** AC susceptibility measurements done under 3.5 Oe/83 Hz AC field. The three samples exhibit a sharp out of phases signal at low temperature. This indicates a superparamagnetic behavior with a blocking temperature ($T_B$) in the range 5–6.4 K.

surface of ZnO decreases the defects amount in ZnO nanorods and enhances its UV photoluminescence. Along with this excellent optical property, the as-obtained nano-composites exhibit a superparamagnetic character with a very low blocking temperature due to the very weak dipolar interactions between the well separated nanoparticles forming the monolayer.


## Acknowledgements

We want to thank the France–Tunisia institute of Cooperation Research Program for its financial support and P. Aschehoug (Laboratoire de Chimie de la matière condensée Chimie Paristech) for the PL analysis.


## References


[1] M.A. Garcia, J.M. Merino, E. Fernandez Pinel, A. Quesada, J. de la Venta, M.L. Ruiz Gonzalez, G.R. Castro, P. Crespo, J. Liopis, J.M. Gonzalez-Calbet, A. Hernando, Nano Lett. 7 (2007) 1489–1494.
[2] G. Kunming, T. Jiaoning, L. Junqin, Y. Qinpeng, Solid State Commun. 139 (2006) 259–262.
[3] T. Wakano, N. Fujimura, Y. Morinaga, N. Abe, A. Ashida, T. Ito, Physica E: Low-Dimens. Syst. Nanostruct. 10 (2001) 260–264.
[4] R. Turgeman, S. Tirosh, A. Gedanken, Chem. – A Eur. J. 10 (2004) 1845–1850.
[5] H. Kim, M. Achermann, L.P. Balet, J.A. Hollingsworth, V.I. Klimov, J. Am. Chem. Soc. 127 (2004) 544–546.
[6] J. Bao, W. Chen, T. Liu, Y. Zhu, P. Jin, L. Wang, J. Liu, Y. Wei, Y. Li, ACS Nano 1 (2007) 293–298.
[7] S.-Y. Yu, H.-J. Zhang, J.-B. Yu, C. Wang, L.-N. Sun, W.-D. Shi, Langmuir 23 (2007) 7836–7840.
[8] Z.H. Zhou, J.M. Xue, H.S.O. Chan, J. Wang, J. Appl. Phys. 90 (2001) 4169–4174.
[9] X. Cao, X. Lan, Y. Guo, C. Zhao, S. Han, J. Wang, Q. Zhao, J. Phys. Chem. C 111 (2007) 18958–18964.
[10] X.Y. Chu, X. Hong, X.T. Zhang, P. Zou, Y.C. Liu, J. Phys. Chem. C 112 (2008) 15980–15984.
[11] P. Wu, N. Du, H. Zhang, L. Jin, D. Yang, Mater. Chem. Phys. 124 (2010) 908–911.
[12] R.Y. Hong, S.Z. Zhang, G.Q. Di, H.Z. Li, Y. Zheng, J. Ding, D.G. Wei, Mater. Res. Bull. 43 (2008) 2457–2468.
[13] S. Si, C. Li, X. Wang, Q. Peng, Y. Li, Sens. Actuat. B: Chem. 119 (2006) 52–56.
[14] J. Cao, W. Fu, H. Yang, Q. Yu, Y. Zhang, S. Wang, H. Zhao, Y. Sui, X. Zhou, W. Zhao, Y. Leng, H. Zhao, H. Chen, X. Qi, Mater. Sci. Eng. B 175 (2010) 56–59.
[15] J. Wan, H. Li, K. Chen, Mater. Chem. Phys. 114 (2009) 30–32.
[16] H. Zhang, D. Yang, X. Ma, N. Du, J. Wu, D. Que, J. Phys. Chem. B 110 (2006) 827–830.
[17] http://www.crystalimpact.com/match/default.htm.
[18] H. Rietveld, Acta Crystallogr. 22 (1967) 151–152.
[19] C.J. Rodriguez, Fullproff, Collected abstract of powder diffraction meeting.
[20] R.M. Cornell, U. Schwertmann, The Iron Oxides: Structure, Properties, Reactions, Occurrence and Uses, VCH, Weinheim, 1996.
[21] N.S. McIntyre, D.G. Zetaruk, Anal. Chem. – A Eur. J. 49 (1977) 1521–1529.
[22] T. Fujii, F.M.F. de Groot, G.A. Sawatzky, F.C. Voogt, T. Hibma, K. Okada, Phys. Rev. B 59 (1999) 3195–3202.
[23] A. Dakhlaoui, M. Jendoubi, L.S. Smiri, A. Kanaev, N. Jouini, J. Cryst. Growth 311 (2009) 3989–3996.
[24] E.G. Bylander, J. Appl. Phys. 49 (1978) 1188–1196.
[25] B. Lin, Z. Fu, Y. Jia, Appl. Phys. Lett. 79 (2001) 943–945.
[26] U. Ozgur, Y.I. Alivov, C. Liu, A. Teke, M.A. Reshchikov, S. Dogan, V. Avrutin, S.J. Cho, H. Morkoc, J. Appl. Phys. 98 (2005) 041301–041403.
[27] K. Vanheusden, W.L. Warren, C.H. Seager, D.R. Tallant, J.A. Voigt, B.E. Gnade, J. Appl. Phys. 79 (1996) 7983–7990.
[28] S. Kumar, B.H. Koo, C.G. Lee, S. Gautam, K.H. Chae, S.K. Sharma, M. Knobel, Funct. Mater. Lett. 04 (2011) 17–20.
[29] J. Li, D. Zhao, X. Meng, Z. Zhang, J. Zhang, D. Shen, Y. Lu, X. Fan, J. Phys. Chem. B 110 (2006) 14685–14687.
[30] F. Chen, R. Shi, Y. Xue, L. Chen, Q.-H. Wan, J. Magn. Magn. Mater. 322 (2010) 2439–2445.
[31] S. Ammar, N. Jouini, F. Fiévet, Z. Beji, L. Smiri, P. Molinié, M. Danot, J.-M. Grenèche, J. Phys.: Condens. Matter 18 (2006) 9055–9069.
[32] C.J. Serna, F. Bodker, S. Morup, M.P. Morales, F. Sandiumenge, S. Veintemillas-Verdaguer, Solid State Commun. 118 (2001) 437–440.
[33] K. Nadeem, H. Krenn, T. Traussnig, R. Wurschum, D.V. Szabo, I. Letofsky-Papst, J. Magn. Magn. Mater. 323 (2011) 1998–2004.
[34] S. Lamba, S. Annapoorni, Eur. Phys. J. B39 (2004) 19–25.
[35] S. Morup, E. Tronc, Phys. Rev. Lett. 72 (1994) 3278–3281.